Progress In Electromagnetics Research, PIER 87, 183–196, 2008

AN EXTENDED FDTD METHOD FOR THE ANALYSIS OF ELECTROMAGNETIC FIELD ROTATIONS AND CLOAKING DEVICES

J. A. Silva-Macêdo, M. A. Romero, and B.-H. V. Borges

Department of Electrical Engineering
School of Engineering of São Carlos
Av. Trabalhador Sãocarlense, 400, 13566-590, São Carlos, SP, Brazil

Abstract—This paper presents a dispersive finite difference time domain (FDTD) method suitable for the analysis of electromagnetic field rotator (and cloaking) devices. The method employs a coordinate transformation which accurately accounts for the radial dependence of the permittivity and permeability tensors, with Drude material models applied to the respective diagonal elements. The key aspect of the present formulation is the inclusion of the radial dependence of the plasma frequency, which makes this formalism quite attractive for the modeling of a general class of cloaking and field rotator geometries. Firstly, the method is validated by comparing its results with a previously published simulation of a cloaking device. Then, it is applied for the first time to the analysis of dispersive effects on the performance of field rotators.

1. INTRODUCTION

The modeling of media capable of bending an incoming wave front around a certain object, followed by a perfect reconstruction of the wave initial profile as it leaves the object, has gained a considerable impulse since the seminal paper by Pendry et al. in 2006 [1]. In this paper, the authors obtained the distortion of the electromagnetic field via coordinate transformation (CT) which was then utilized to generate electric permittivity (ε) and magnetic permeability (μ) values. Later that year, the predictions described in [1] were experimentally verified by Schurig et al. [2] who presented the first practical realization of a cloaking device operating in the microwave region with striking repercussions in the scientific community. A crucial requirement for the cloaking effect to take place is a precise control of the medium

properties in such way to prevent the scattering of the incident wave front. Hence, design and modeling of the cloaking process requires a careful mapping of the medium properties, via CT. For example, in [1] a given free space region is mapped into a spherical volume with anisotropic and spatially varying ε and μ. An accurate CT description of material properties for spaces with either spherical or cylindrical holes inside them can be found in [3]. In addition, the sensitivity of spherical and cylindrical transformation cloaks to non-ideal factors in the fabrication process has been properly investigated in [4].

CT has also been the preferred tool for the design of devices just as remarkable as the invisibility cloaks, such as hiperlenses [5, 6] (where coordinate transformation is utilized for the calculation of electromagnetic parameters aiming at obtaining perfect lenses and superlenses), field concentrators [7–9] (where the electromagnetic parameters are calculated in such a way as to confine the incident radiation), and field rotators [9, 10] (a transformation media capable of rotating the wave front of an electromagnetic wave by a predetermined angle). Recently, Chen et al. [11] have investigated a transformation medium aiming at extending the bandwidth of an invisibility cloak. To do so, the frequency dispersion of the metamaterial was taken into account through a Lorentz material model, resulting in a dispersive cloak. Dispersive approaches based on the two-dimensional finite difference time domain (2D-FDTD) method have been suggested simultaneously by us [12] and [13, 14] for the analysis of cloaking applications. In both cases, the dispersive nature of the materials was accounted for in terms of the Drude material model.

Here, we present an extended 2D-FDTD formulation which can be employed for the simulation of electromagnetic field rotators and cloaking devices, as originally introduced in [12]. This approach accurately takes into account the dispersive nature of the constituent materials. An important aspect of the present formulation is the inclusion of the radial dependence of the plasma frequency, which makes this formalism quite attractive for the modeling of a general class of cloaking and field rotator geometries. In addition, the present formalism easily incorporates all elements of the permittivity and permeability tensors. The mapped material coordinate transformation for $\varepsilon(\omega)$ and $\mu(\omega)$ are described in terms of Drude models, which are applied to the respective diagonal elements.

Also, we carry out an investigation concerning how the dispersive nature of the constituent materials affects the response of electromagnetic field rotators. To the best of our knowledge, it is the first time that results like those are reported in the literature.

The paper is organized as follows. Section 2 describes the FDTD

formalism utilized in the simulations. Next, Section 3 presents some relevant results followed by some concluding remarks in Section 4.

2. THEORY

The structure investigated in this work is schematically depicted in Fig. 1, defined in Cartesian coordinates. The goal is to develop a formalism capable of simulating a general class of dispersive media [12]. If necessary, higher order FDTD schemes, such as the one proposed in [15], could be successfully employed in this expansion as well. We consider the whole medium in the computational domain as being described by the Drude material model. The Maxwell equations assuming TE_z polarized waves (E_x, E_y and H_z), are written as

$$\frac{\partial D_x}{\partial t} = \frac{\partial H_z}{\partial y} \tag{1}$$

$$\frac{\partial D_y}{\partial t} = -\frac{\partial H_z}{\partial x} \tag{2}$$

$$\frac{\partial B_z}{\partial t} = \frac{\partial E_x}{\partial y} - \frac{\partial E_y}{\partial x} \tag{3}$$

The permittivity and permeability parameters of the media, responsible for the rotation of the electromagnetic field, are spatially dependent and biaxially anisotropic, and obtained via CT according to [10]. To do so, we consider the electric displacement vector $\overline{D}$ and the magnetic flux density $\overline{B}$, as follows

$$\overline{D} = \varepsilon_0 \overline{\overline{\varepsilon}}_r \cdot \overline{E} \quad \text{and} \quad \overline{B} = \mu_0 \overline{\overline{\mu}}_r \cdot \overline{H},$$

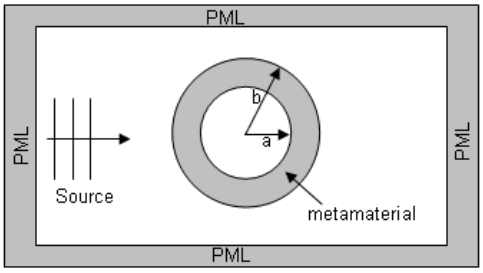

Figure 1. Computational domain for the field rotator [10].

where

$$\overline{\overline{\varepsilon}}_r = \overline{\overline{\mu}}_r = \begin{bmatrix} c_{11} & c_{12} & c_{13} \\ c_{21} & c_{22} & c_{23} \\ c_{31} & c_{32} & c_{33} \end{bmatrix} \tag{4}$$

To obtain the elements c_{ij} $(i,j=1,2,3)$, we start with the Jacobian matrix, relating the transformed with the original coordinate as follows:

$$\Lambda_{\alpha}^{\alpha'} = \frac{\partial x^{\alpha'}}{\partial x^{\alpha}}. \tag{5}$$

The permittivity and permeability tensor components of the transformed medium are obtained according to

$$\varepsilon_r^{i'j'} = \mu_r^{i'j'} = \left|\det\left(\Lambda_{\alpha}^{\alpha'}\right)\right|^{-1} \Lambda_i^{i'} \Lambda_j^{j'} \tag{6}$$

As in [9], the coordinate transformation obeys the following relations (see Fig. 1):

$r' = r,\ \theta' = \theta$ and $z' = z$, for $r > b$,
$r' = r,\ \theta' = \theta + \theta_0$ and $z' = z$, for $r < a$,
$r' = r,\ \theta' = \theta + \theta_0[f(b) - f(r)]/[f(b) - f(a)]$ and $z' = z$, for $a < r < b$,

where $f(r)$ is any continuous function of r (where $r^2 = x^2 + y^2$). This transformation rotates the cylinder from an angle $\theta = 0$ at $r = b$ up to $\theta = \theta_0$ at $r = a$. By using (5)–(6) one finds the following relations for the relative permittivity and permeability tensor components between $a \leq r \leq b$, which are given here for completeness

$$\begin{aligned} c_{11} &= 1 + 2t\cos\theta\sin\theta + t^2\sin\theta, \\ c_{12} &= c_{21} = -t^2\cos\theta\sin\theta - t\left(\cos^2\theta - \sin^2\theta\right), \\ c_{22} &= 1 - 2t\cos\theta\sin\theta + t^2\cos\theta, \\ c_{23} &= c_{32} = 0,\ \ c_{33} = 1,\ \text{ and }\ t = \frac{\theta_0 r f'(r)}{f(b) - f(a)}. \end{aligned}$$

The Drude material model is included in this formalism by making use of the electric polarization vector, which allows the components of the relative permittivity tensor to be written as

$$\varepsilon_{xx} = \varepsilon_0(\varepsilon_{\infty x} + \chi_{xx}), \tag{7}$$
$$\varepsilon_{xy} = \varepsilon_0 c_{12}, \tag{8}$$
$$\varepsilon_{yy} = \varepsilon_0(\varepsilon_{\infty y} + \chi_{yy}), \tag{9}$$
$$\varepsilon_{yx} = \varepsilon_0 c_{21}, \tag{10}$$

where χ_{mm} $(m, n = x, y)$ are the susceptibility tensor components and $\varepsilon_{\infty x,y}$ is the electric permittivity at infinite frequency. The susceptibility tensor components are represented in terms of the Drude model according to

$$\chi(\omega) = -\frac{\omega_p^2}{\omega + j\omega\Gamma}, \tag{11}$$

where ω_p is the plasma frequency and Γ is the damping factor. Observe that only the diagonal terms of the relative permittivity tensor are expressed in terms of the Drude model, Equations (7) and (9). In the present case, where TE_z polarization has been assumed, the relative permeability tensor will be $\overline{\overline{\mu}}_r = [I]$ (where I is the identity matrix), in the whole computational domain. In the next examples, the damping factor will be assumed as zero, without loss of generality. At this point it is important to emphasize that the plasma frequency for the rotating coating (cylinder) is now a function of position, and therefore it needs to be calculated for each tensor component. For example, ω_p for the tensor component ε_{xx} (Equation (7)) is obtained by noticing that $\varepsilon_0 c_{11} = \varepsilon_{xx}$, which gives

$$\varepsilon_{\infty x} + \chi_{xx} = c_{11}.$$

Using (11) in the above equation, with the assumption that $\Gamma = 0$, one obtains $\omega_{px} = \omega\sqrt{\varepsilon_{\infty x} - c_{11}}$. This equation clearly shows a spatial dependency, since c_{11} is a function of r through the variable t. The expression for ω_{py} is obtained in an analogous fashion, resulting in $\omega_{py} = \omega\sqrt{\varepsilon_{\infty y} - c_{22}}$, which is also a function of r.

Next, we expand (1)–(2) with the help of (7)–(11), which gives

$$\frac{\partial D_x}{\partial t} = \varepsilon_0\varepsilon_{\infty x}\frac{\partial E_x}{\partial t} + J_x + \varepsilon_{xy}\frac{\partial E_y}{\partial t} = \frac{\partial H_z}{\partial y}, \tag{12}$$

$$\frac{\partial D_y}{\partial t} = \varepsilon_{yx}\frac{\partial E_x}{\partial t} + \varepsilon_0\varepsilon_{\infty y}\frac{\partial E_y}{\partial t} + J_y = -\frac{\partial H_z}{\partial x}, \tag{13}$$

where J_x and J_y are the components of the surface current density in the x and y directions, respectively, given by

$$\frac{\partial J_{x,\,y}}{\partial t} = \varepsilon_0\omega_{px,\,py}^2 E_{x,\,y}.$$

After some algebraic manipulations of (12) and (13) one arrives at the following differential equations for the E_x and E_y components

$$\frac{\partial E_x}{\partial t} = \left[\varepsilon_0\varepsilon_{\infty y}\frac{\partial H_z}{\partial y} + \varepsilon_{xy}\frac{\partial H_z}{\partial x} + \varepsilon_{xy}J_y - \varepsilon_0\varepsilon_{\infty y}J_x\right]$$

$$/\left[\varepsilon_0^2\varepsilon_{\infty y}\varepsilon_{\infty x} - \varepsilon_{xy}\varepsilon_{yx}\right] \tag{14}$$

$$\frac{\partial E_y}{\partial t} = -\left[\varepsilon_0\varepsilon_{\infty x}\frac{\partial H_z}{\partial x} + \varepsilon_{yx}\frac{\partial H_z}{\partial y} + \varepsilon_{yx}J_x + \varepsilon_0\varepsilon_{\infty x}J_y\right] \left[\varepsilon_0^2\varepsilon_{\infty x}\varepsilon_{\infty y} - \varepsilon_{yx}\varepsilon_{xy}\right] \tag{15}$$

The expansion for the H_z component is obtained directly from (3). Therefore, the updating equations in finite differences can be written as follows,

$$\begin{aligned}
E_x^{i-1/2}(m,n) &= E_x^{i-1/2}(m,n) + \frac{\Delta t}{\left[\varepsilon_0^2 A\varepsilon_{\infty x}(m,n) - B\varepsilon_{yx}(m,n)\right]} \\
&\quad \cdot \left[\varepsilon_0 A\frac{\left[H_z^i(m,n+1) - H_z^i(m,n)\right]}{\Delta y}\right. \\
&\quad \left. + B * C + B * D - \varepsilon_0 A * E\right] \\
E_y^{i+1/2}(m,n) &= E_y^{i-1/2}(m,n) - \frac{\Delta t}{\left[\varepsilon_0^2 F\varepsilon_{\infty y}(m,n) - G\varepsilon_{xy}(m,n)\right]} \\
&\quad \cdot \left[\varepsilon_0 F\frac{\left[H_z^i(m+1,n) - H_z^i(m,n)\right]}{\Delta x}\right. \\
&\quad \left. + G * H + G * I + \varepsilon_0 F * J\right] \\
J_x^{i+1}(m,n) &= J_x^i(m,n) + \frac{\varepsilon_0\omega_{px}^2(m,n)\Delta t}{2} \\
&\quad \left[E_x^{i+1/2}(m,n) + E_x^{i+1/2}(m+1,n)\right] \\
J_y^{i+1}(m,n) &= J_y^i(m,n) + \frac{\varepsilon_0\omega_{py}^2(m,n)\Delta t}{2} \\
&\quad \left[E_y^{i+1/2}(m,n) + E_y^{i+1/2}(m,n+1)\right] \\
H_z^{i+1}(m,n) &= H_z^i(m,n) + \frac{\mu_0\left[E_x^{i+1/2}(m,n) - E_x^{i+1/2}(m,n-1)\right]}{\Delta y} \\
&\quad - \frac{\mu_0\left[E_y^{i+1/2}(m,n) - E_y^{i+1/2}(m-1,n)\right]}{\Delta x}
\end{aligned}$$

with

$$\begin{aligned}
A &= 0.25\left[\varepsilon_{\infty y}(m,n) + \varepsilon_{\infty y}(m-1,n)\right. \\
&\quad \left. + \varepsilon_{\infty y}(m-1,n+1) + \varepsilon_{\infty y}(m,n+1)\right], \\
B &= 0.25\left[\varepsilon_{xy}(m,n) + \varepsilon_{xy}(m-1,n)\right.
\end{aligned}$$

$$
\begin{aligned}
&+\varepsilon_{xy}(m-1,n+1)+\varepsilon_{xy}(m,n+1)\big]\,,\\
C &= \frac{0.25}{\Delta x}\Big[H_z^i(m+1,n)-H_z^i(m-1,n)\\
&+H_z^i(m+1,n+1)-H_z^i(m-1,n+1)\Big]\,,\\
D &= 0.5\Big[J_x^i(m,n)+J_x^i(m-1,n)\Big]\,,\\
E &= 0.5\Big[J_y^i(m,n)+J_y^i(m-1,n)\Big]\,,\\
F &= 0.25\left[\varepsilon_{\infty x}(m,n)+\varepsilon_{\infty x}(m,n+1)\right.\\
&\left.+\varepsilon_{\infty x}(m-1,n)+\varepsilon_{\infty x}(m-1,n+1)\right]\,,\\
G &= 0.25\left[\varepsilon_{yx}(m,n)+\varepsilon_{yx}(m,n+1)\right.\\
&\left.+\varepsilon_{yx}(m-1,n)+\varepsilon_{yx}(m-1,n+1)\right]\,,\\
H &= \frac{0.25}{\Delta y}\Big[H_z^i(m,n+1)-H_z^i(m,n-1)\\
&+H_z^i(m+1,n+1)-H_z^i(m+1,n-1)\Big]\,,\\
I &= 0.5\Big[J_x^i(m,n)+J_x^i(m,n-1)\Big]\,,\\
J &= 0.5\Big[J_y^i(m,n)+J_y^i(m,n-1)\Big]\,.
\end{aligned}
$$

A similar expansion can be obtained for TM_z polarized waves in terms of magnetic flux density $\overline{B}$. The pertinent equations are

$$
\begin{aligned}
\frac{\partial B_x}{\partial t} &= \mu_{xx}\frac{\partial H_x}{\partial t}+\mu_{xy}\frac{\partial H_y}{\partial t}=-\frac{\partial E_z}{\partial y},\\
\frac{\partial B_y}{\partial t} &= \mu_{yx}\frac{\partial H_x}{\partial t}+\mu_{yy}\frac{\partial H_y}{\partial t}=\frac{\partial E_z}{\partial x},\\
\frac{\partial D_z}{\partial t} &= \varepsilon_z\frac{\partial E_z}{\partial t}=\left[\frac{\partial H_y}{\partial x}-\frac{\partial H_x}{\partial y}\right].
\end{aligned}
$$

The finite difference expansion of these equations is lengthy but straightforward, and will be omitted here. The next section presents some numerical results for the structure described in Fig. 1.

3. RESULTS

Before we start the analysis of the field rotator structure, it becomes important to properly validate the theory introduced in the previous section. An interesting way of stressing this method consists in analyzing an invisibility cloaking device, such as the one proposed in [2]. The structure is essentially the same one depicted in Fig. 1

Table 1. Pertinent parameters for the simulation of the cloaking device.

Parameter	Value
$N_x \times N_y$	2200×2200
Δ_x (mm)	0.05
Δ_y (mm)	0.05
Δ_t (ps)	0.112
a (mm)	27.00
b (mm)	59.00
N_{PML}	20
$\sigma_{\max}$	$15\,\omega\varepsilon_0$
$N\Delta t$	30000

for the field rotator, and requires that the field must not penetrate in the region $r < a$ and also that no rotation (θ) should occur. The pertinent parameters utilized in this simulation are listed in Table 1. The parameters defined in this table are: the computational domain size (N_x, N_y), the spatial step size (Δ_x, Δ_y), the temporal step size (Δ_t), the inner and out radii of the rotation region (a, b), the number of PML (perfect matched layer) cells (N_{PML}), the maximum conductivity ($\sigma_{\max}$, defined as in [12]), and the number of time steps ($N\Delta t$). The source is sinusoidal with a frequency $f = 8.625\,\text{GHz}$ ($\lambda \approx 34.76\,\text{mm}$) modeled via Total Field/Scattered Field (TFSF) [16]. The dumping factor $\Gamma = 0.01\,\text{GHz}$, throughout the whole cylinder, which matches the experimental value obtained in [2]. The incident wave is assumed as TM_z polarized. The pertinent parameters utilized in this simulation are listed in Table 1. The parameters defined in this table are: the computational domain size (N_x, N_y), the spatial step size ($\Delta_x = \Delta_y \approx \lambda/700$), the temporal step size (Δt) defined in terms of the Courant criteria, the inner and outer radii of the rotation region (a, b), the number of PML (perfect matched layer) cells (NPML), the maximum conductivity ($\sigma_{\max}$, defined as in [16]), and the number of time steps ($N\Delta t$).

For the cloaking device, the following relations are valid:

$$r' = r,\ \theta' = \theta,\ \text{and}\ z' = z\ \text{for}\ r' \geq b,$$

$$r' = \frac{b-a}{b} r + a,\ \theta' = \theta,\ \text{and}\ z' = z\ \text{for}\ a \leq r \leq b.$$

Therefore, one will end up with the following expression for the relative permittivity and permeability,

$$\varepsilon'_r = \mu'_r = \begin{bmatrix} \dfrac{r'-a}{r'}\cos^2\theta + \dfrac{r'}{r'-a}\sin^2\theta & \dfrac{a^2-2r'a}{r'(r'-a)}\cos\theta\sin\theta & 0 \\ \dfrac{a^2-2r'a}{r'(r'-a)}\cos\theta\sin\theta & \dfrac{r'-a}{r'}\sin^2\theta + \dfrac{r'}{r'-a}\cos^2\theta & 0 \\ 0 & 0 & \left(\dfrac{r'-a}{r'}\right)\cdot\left(\dfrac{b}{b-a}\right)^2 \end{bmatrix}.$$

The simulation results for the cloaking device are shown in Fig. 2 in terms of the E_z component. Observe that there is no significant field inside the region $r \leq a$, as one would expect. In addition, the simulation result agrees remarkably well with the experimental ones obtained in [2] for the fabricated cloaking device, which is justified since the present model accurately incorporates the dispersive nature of the materials involved (including the experimental dumping factor). It is worth mentioning at this point that we have not utilized a radial-dependent dumping factor as is done in [14]. Here, Γ is constant throughout the cylinder. Therefore, it is expected for the present case that the wave should experience additional perturbations as it propagates through the cylinder.

Next, we investigate the field rotator based on the structure illustrated in Fig. 1. The constitutive parameters were obtained through CT in which the rotating coating is assumed as immersed in free space and phase matched to this medium at the operating frequency $f = 1.0\,\mathrm{GHz}$. As in the previous example, the edges of the computational window are terminated with PML, whose maximum conductivity is also defined as in [16]. All pertinent simulation parameters are listed in Table 2. The source used in these simulations is a plane wave implemented using the Total Field/Scattered Field technique [16]. The wave in this case is assumed as TE_z polarized.

The field distribution for the H_z component is given in Fig. 3. Observe that a small perturbation in the wave front can still be observed after it leaves the field rotator. This is somewhat expected, given that the external media (air) has a plasma frequency $\omega_p = 0$, making it difficult to precisely match the impedance between external and rotated media.

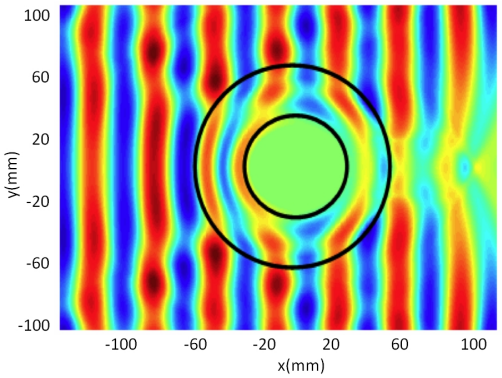

Figure 2. Field distribution for the E_z component obtained for the cloaking device. The source frequency is 8.625 GHz, and the dumping factor is $\Gamma = 0.01$ GHz. Simulation parameters are provided in Table 1.

Table 2. Pertinent parameters utilized in the simulation of the field rotator device.

Parameter	**Value**
$N_x \times N_y$	600×600
Δ_x (m)	0.25
Δ_y (m)	0.25
Δ_t (ps)	0.56
a (m)	0.25
b (m)	0.50
N_{PML}	10
$\sigma_{\max}$	$15(2\pi f_0)$
$N\Delta t$	8000

We have also simulated how small variations in the excitation conditions can affect the performance of the field rotator. To do so, we have arbitrarily chosen two distinct frequencies for the incident field, namely, 0.9 GHz and 1.02 GHz. The simulated results for both cases can be seen in Figs. 4(a) and (b), respectively, which shows the field distribution for the H_z component, obtained after 8000 time steps. As expected, the electromagnetic pattern becomes significantly

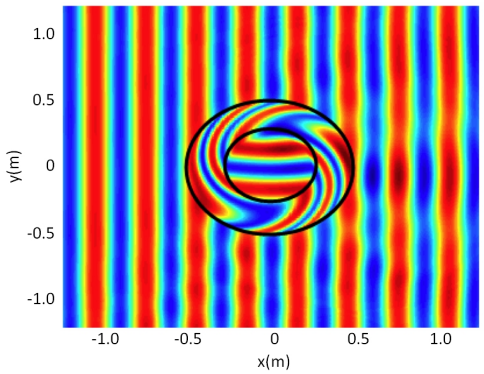

Figure 3. Magnetic field distribution for the H_z component obtained for the field rotator device. The designed central frequency $f = 1.0\,\text{GHz}$.

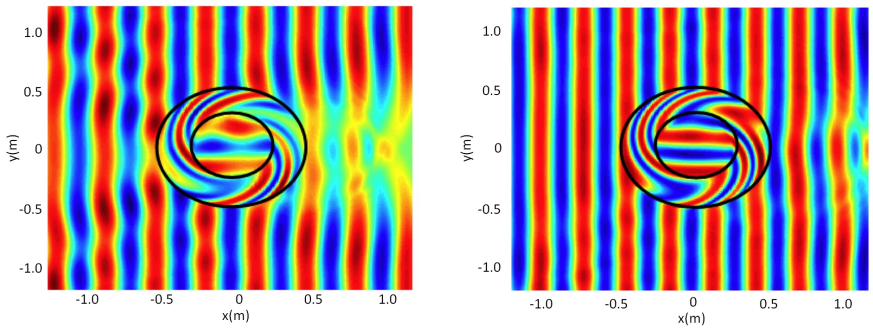

(a) (b)

Figure 4. Magnetic field distribution for the H_z component obtained for the field rotator device. Incident wave with (a) $f = 0.9\,\text{GHz}$, and (b) $f = 1.02\,\text{GHz}$.

affected even by small changes around the excitation condition. This is a strong indication of how sensitive the transformation media can be with respect to the design parameters. We take this aspect a step further and investigate the scattering cross section (SCS) for different excitation frequencies (normalized to the designed frequency), as shown in Fig. 5. The smallest cross section, as expected, is for the design frequency of 1 GHz. Nonetheless, the low values of SCS observed at frequency values different from the designed one are necessarily not an indication that the field rotator can operate efficiently at these frequencies as well (such as $\sim 0.87\,\text{GHz}$ and $\sim 1.2\,\text{GHz}$, for example).

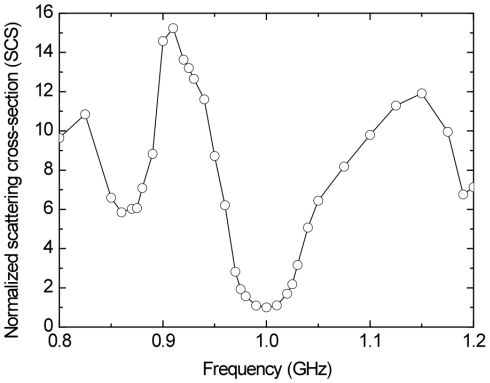

Figure 5. Normalized scattering cross section as function of the frequency for the dispersive filed rotator.

The reason is due to the impedance mismatch that will cause a significant perturbation in the field as it leaves the rotator for these frequencies.

Other configurations for the field rotator will be considered in future publications. We expect to address issues such as rotator geometry and dispersive external media, and how these parameters influence the overall performance of the device. This will enable us to study more accurately aspects of impedance matching as well as to explore the wide-band nature of the proposed formalism.

4. CONCLUSION

We have implemented a dispersive 2D-FDTD formalism that can be applied to the modeling of field rotators as well as electromagnetic cloaking devices. The method employs a coordinate transformation which accurately accounts for the radial dependence of the permittivity and permeability tensors, with Drude material models applied to the respective diagonal elements. The proposed model also incorporates the radial dependence of the plasma frequency, which makes this formalism quite attractive for the modeling of a general class of cloaking and field rotator geometries. We have applied this method for the first time to the analysis of dispersive effects on field rotators and showed that the performance of these structures can be severely affected if they are not operated on the designed frequency.

ACKNOWLEDGMENT

The authors would like to acknowledge the financial support from FAPESP, CNPq, and CAPES.

REFERENCES

1. Pendry, J. B., D. Schurig, and D. R. Smith, "Controlling electromagnetic fields," *Science*, Vol. 312, 1780–1782, June 2006.
2. Schurig, D., J. J. Mock, B. J. Justice, S. A. Cummer, J. B. Pendry, A. F. Starr, and D. R. Smith, "Metamaterial electromagnetic cloak at microwave frequencies," *Science*, Vol. 314, 977–980, Nov. 2006.
3. Schurig, D., J. B. Pendry, and D. R. Smith, "Calculation of material properties and ray tracing in transformation media," *Opt. Express*, Vol. 14, 9794–9804, Oct. 2006.
4. Zhang, J. J., Y. Luo, H.S. Chen, and B.-I. Wu, "Sensitivity of transformation cloak in engineering," *Progress In Electromagnetics Research*, PIER 84, 93–104, 2008.
5. Tsang, M. and D. Psaltis, "Magnifying perfect lens and superlens design by coordinate transformation," *Phys. Rev. B*, Vol. 77, 035122, 2008.
6. Kildishev, A. V. and E. E. Narimanov, "Impedance-matched hyperlens," *Opt. Letters*, Vol. 32, 3432–3434, Nov. 2007.
7. Rahm M., D. Schurig, D. A. Roberts, S. A. Cummer, D. R. Smith, and J. B. Pendry, "Design of electromagnetic cloaks and concentrators using form-invariant coordinate transformations of Maxwell's equations," *Phot. Nanostruc. Fund. and Appl.*, Vol. 6, 87–95, Aug. 2007.
8. Yaghjian, A. D. and S. Maci, "Alternative derivation of electromagnetic cloaks and concentrators," arXiv:0710.2933, 2007 (unpublished).
9. Luo, Y., H. Chen, J. Zhang, L. Ran, and J. A. Kong, "Design and analytical full-wave validation of the invisibility cloaks, concentrators, and field rotators created with a general class of transformations," *Phys. Rev. Appl.*, Vol. 77, 125127/1–125127/8, Mar. 2008.
10. Chen, H. and C. T. Chan, "Transformation media that rotate electromagnetic fields," *Appl. Phys. Letters*, Vol. 90, 241105/1–241105/3, June 2007.
11. Chen, H., Z. Liang, P. Yao, X. Jiang, H. Ma, and C. T. Chan,

"Extending the bandwidth of electromagnetic cloaks," *Phys. Review B*, Vol. 76, 241104/1–241104/4, Dec. 2007.

12. Silva-Macêdo, J. A., M. A. Romero, and B.-H. V. Borges, "Improved FDTD formalism for electromagnetic cloaking applications," *13th IEEE Conference on Electromagnetic Field Computation — CEFC 2008*, 464, Athens, Greece, May 11–15, 2008.
13. Zhao, Y., C. Argyropoulos, and H. Yang, "Dispersive finite-difference time-domain simulation of electromagnetic cloaking devices," *Antennas and Propagation Conference, 2008. LAPC 2008. Loughborough*, 429–432, March 17–18, 2008.
14. Argyropoulos, C., Y. Zhao, and Y. Hao, "A radial-dependent dispersive finite-difference time-domain method for evaluation of electromagnetic cloaks," arXiv:0805.2050v1, May 14, 2008.
15. Prokopidis, K. P., E. P. Kosmidou, and T. D. Tsiboukis, "An FDTD algorithm for wave propagation in dispersive media using higher-order schemes," *J. Electromagn. Waves Applicat.*, Vol. 18, No. 9, 1171–1194, 2004.
16. Taflove, A. and S. C. Hagness, *Computational Electrodynamics the Finite-difference Time Domain Method*, Artech House, Norwood, 2005.